Guided Subdivision

K. Karčiauskas and J. Peters

June 29, 2005

Abstract

Curvature continuous surfaces with subdivision structure are constructed by higher-order sampling of a piecewise polynomial guide surface, at positions defined and derivatives weighted by a special, scalable reparametrization. Two variants are developed. One variant applies to the conventional sprocket subdivision layout, say of Catmull-Clark subdivision, i.e. nested rings consisting of N copies of L-shaped segments with three patches. The curvature continuous surfaces are of degree (6,6). A second variant, called polar guided subdivision, is particularly suitable for high valences N and to cap cylindrical structures. It yields curvature continuous surfaces of degree (4,3). Additionally, we discuss a scheme that samples with increasing density to generate a C^2 surface of piecewise degree (3,3). Curvature continuity is verified by showing convergence of anchored osculation paraboloids.

1 Introduction

Guided subdivision is a stationary subdivision procedure capable of generating, in principle arbitrarily smooth, surfaces by sampling the composition of a *guide surface* with a *scalable reparametrization*. While the guide surface captures the shape implied by pre-existing data, the reparametrization is crucial to orient and scale higher-order derivatives taken off the guide surface. While just about any guide surface representation works, e.g. rational or the polynomial constructions of [Pra97, Rei98], we choose a piecewise polynomial guide to get good shape reproduction at low degree. In contrast to [Pra97, Rei98], the composition of guide and reparametrization is not used directly but *sampled*. This allows us to use the economy of spline constructions to trade more pieces for reduced polynomial degree. Applying several steps of guided subdivision before capping with

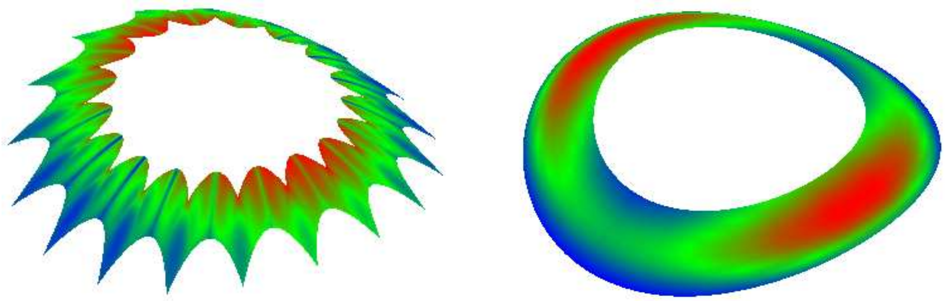

Figure 1: Gauss-curvature-colored subdivision surface ring consisting of 18 segments for (*left*) sprocket (Ger. Zahnkranz) layout of Catmull-Clark subdivision, (*right*) polar layout.

polynomial pieces is an important ingredient in the construction of high-quality multi-sided surface blends, explained in the sequel [KP0x] to this paper, since guided subdivision surface rings introduce fewer shape and curvature artifacts than an equal number of conventional subdivision rings depending only on the input mesh without guide. The publication [KP0x] also explains how guide surfaces are derived from boundary data. In the present paper, the guide surface is assumed to be given so that only its structure needs to be explained.

A key new contribution of this paper is the introduction of *polar guided subdivision*. Polar subdivision has a different patch layout than the conventional sprocket-shaped arrangement of N L-shaped segments (Figure 1). While the basic structure of subdivision is the same in both layouts, the quadrilateral domain pieces, from which the underlying topological space is built, are glued together differently. This polar layout is particularly suitable for modeling high valence configurations and allows for polynomial subdivision surfaces of lower degree, namely (4,3), to achieve curvature continuity.

At first sight, guided subdivision appears to be more complex than subdivision based on the control mesh alone. However, guided subdivision is a *stationary* procedure that matches the structure of subdivision as laid out e.g. in [RP05]. Guided subdivision is also a stable procedure. Due to the guide surface, the proof of smoothness at the extraordinary point, i.e. the limit point where $N \neq 4$ surface segment meet, is simpler than for conventional subdivision. Our proof is based on showing convergence of a sequence of *anchored osculating paraboloids* (local quadratic functions over the tangent plane). This allows us to *quantify deviation from curvature continuity* when using constructions of degree lower than (6,6) in the sprocket layout, respectively (4,3) in the polar layout.

Guided subdivision is explained in the following steps.
Section 2 defines the layout of the guided subdivision patches (sprocket or polar).
Section 3 defines scalable reparametrizations ρ.
Section 4 defines the C^2 guide spline $\mathbf{g}$ whose free parameters can be set to match boundary data.
Section 5 defines the patches $\mathbf{x}_n^m := H(\mathbf{g}_n \circ \rho_n^m)$ as Hermite interpolant of the composition of the nth piece of the guide surface $\mathbf{g}$ with the nth piece of the m-times refined reparametrization ρ. This defines the guided subdivision.
Section 6 assembles the pieces $\mathbf{x}_n^m$ into surface rings $\mathbf{x}^m$; a union of rings forms a C^2 (G^2) guided patchwork.
Section 7 analyzes the infinite union of surface rings, i.e. it characterizes guided subdivision.
Section 8 provides curvature estimates for guided subdivision of lower degree than is needed for curvature continuity, with the help of anchored osculating paraboloids.
Section 9 discusses a modification of guided subdivision, the accelerated bicubic guided C^2 scheme.
Section 10 discusses rational guided subdivision.

2 The structure of guided subdivision surfaces

Locally, a subdivision surface $\mathbf{x} \in \mathbb{R}^d$ is the union of a sequence of nested *surface rings* $\mathbf{x}^m$ converging to an extraordinary or *central point* $\mathbf{x}^{\mathrm{c}}$:

$$\mathbf{x} = \bigcup_{m \in \mathbb{N}} \mathbf{x}^m \cup \mathbf{x}^{\mathrm{c}} .$$

Each surface ring $\mathbf{x}^m$ in turn is the union of N *segments* $\mathbf{x}_n^m$, $n = 0, \ldots, N-1$ (a segment $\mathbf{x}_n^m$ can consist of several Bézier patches):

$$\mathbf{x}^m = \bigcup_{n=0}^{N-1} \mathbf{x}_n^m .$$

The domain $\mathbf{S}^0$ of each ring $\mathbf{x}^m$ is obtained from N copies of a basic domain $\Sigma^0 \subset \mathbb{R}^2$ (see Figures 2(b), 3(b)) by setting edges of (Σ^0, n) and $(\Sigma^0, n+1)$ equal (see Figures 2(c), 3(c)):

$$\mathbf{S}^0 := \Sigma^0 \times \mathbb{Z}_N, \quad \mathbb{Z}_N := \mathbb{Z} \mod N.$$

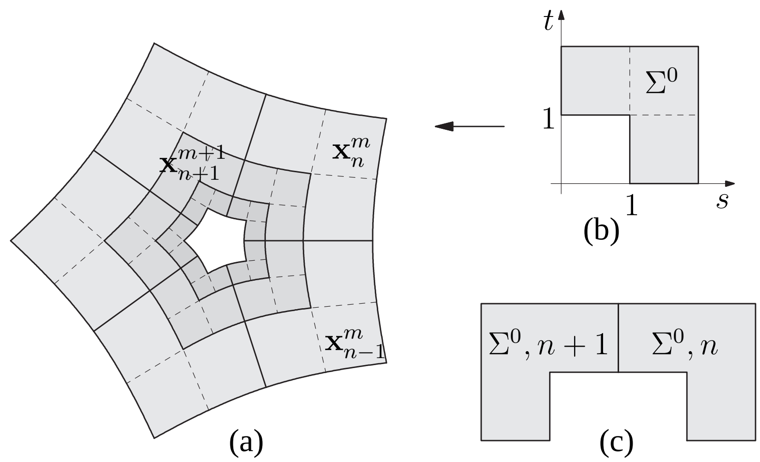

Figure 2: (a) sprocket layout; (b) basic domain Σ^0 ; (c) gluing copies of basic domain to form $\mathbf{S}^0$.

The rings $\mathbf{x}^m$ of guided subdivision are special in that they are constructed by sampling position and derivatives of a *guide* surface g with respect to a parametrization ρ^m that, itself, has subdivision structure (as a map into $\mathbb{R}^d, d = 2$). That is, to define $\mathbf{x}^m$, we Hermite-sample $\mathbf{g} \circ \rho^m$ where

$$\rho^m : \mathbf{S}^0 \to \Omega \subset \mathbb{R}^2, \quad (s, t, n) \mapsto (u, v),$$

$$\mathbf{g} : \Omega \to \mathbb{R}^3, \quad (u, v) \mapsto (x, y, z).$$

We distinguish two cases of reparametrization that differ in their patch layout.
sprocket layout: The basic domain is (Figure 2 (b))

$$\Sigma^0 := [0, 2]^2 \setminus [0, 1)^2 \, .$$

Edges of copies of Σ^0 are set equal according to

$$(0, s, n) = (s, 0, n + 1), \quad s \in [1..2], \; n \in \mathbb{Z}_N \, .$$

The consecutive rings $\mathbf{x}^m$ yield the layout of Figure 2 (a), familiar from the characteristic map of Catmull-Clark subdivision. In the sprocket layout, segments $\mathbf{x}_n^m$ will consist of patches of degree (k, k), i.e. degree k in each variable.
polar layout: The basic domain is (Figure 3 (b))

$$\Sigma^0 := [0..1]^2$$

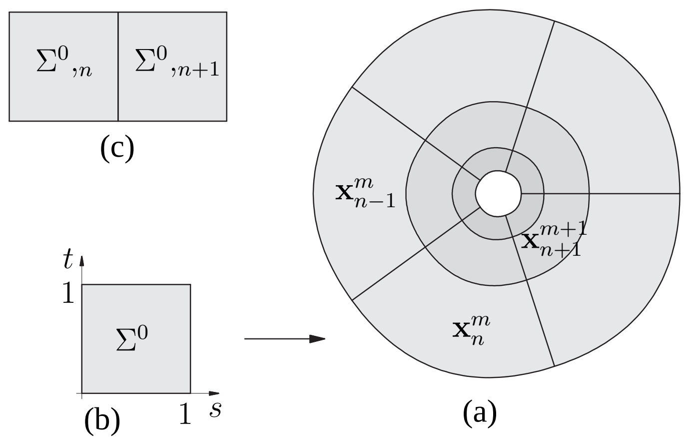

Figure 3: (a) polar layout; (b) basic domain Σ^0 ; (c) gluing copies of basic domain to form $\mathbf{S}^0$.

Edges of copies of Σ^0 are set equal according to

$$(1, t, n) = (0, t, n + 1), \quad t \in [0..1],\ n \in \mathbb{Z}_N.$$

The consecutive rings $\mathbf{x}^m$ yield the layout of Figure 3 (a). In this polar layout, segments $\mathbf{x}^m_n$ consist of patches of degree (degree circular, degree radial); we parametrize the *circular* direction by s and the *radial* direction by t.

3 Scalable reparametrizations

In this section, we describe two maps $\hat{\rho}$ and $\breve{\rho}$ that alternatively define the coordinates in which the guide surface $\mathbf{g}$ is Hermite sampled. They are associated with different patch layouts

sprocket layout: The reparametrization $\hat{\rho}$ is associated with multi-sided gaps in standard spline constructions. It consists of scaled copies of the characteristic map $\hat{\rho}^0$ of Catmull-Clark subdivision (see e.g. [PR98]); $\hat{\rho}^0$ maps N copies of the L-shaped domain Σ^0 in Figure 2 (b) to an annulus or ring in $\mathbb{R}^2$. If we fix scaling and rotation, $\hat{\rho}$ is uniquely determined. The reparametrization $\hat{\rho}^0$ is C^2 and scaling it by

$$\hat{\lambda} := (\mathsf{c} + 5 + \sqrt{(\mathsf{c}+9)(\mathsf{c}+1)})/16, \qquad \mathsf{c} := \cos\alpha, \quad \alpha := 2\pi/N,$$

(the subdominant eigenvalue of the Catmull-Clark subdivision matrix) results in a copy $\hat{\rho}^1$ that joins $\hat{\rho}^0$ C^2 in the same fashion as do rings of a Catmull-Clark

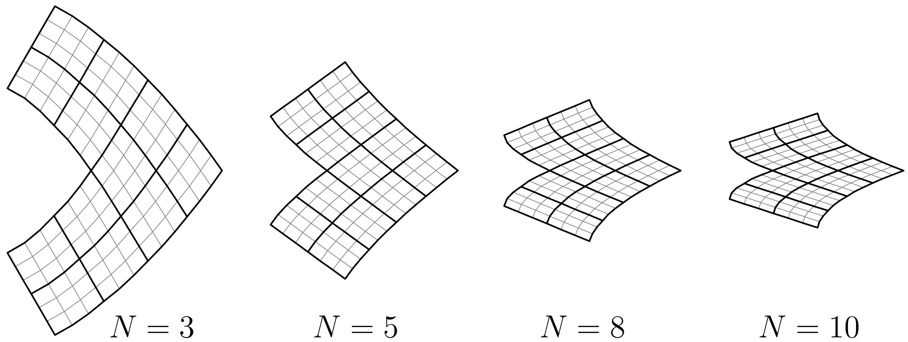

Figure 4: Alternative bicubic C^2 reparametrization scalable by $1/2$.

subdivision surface. (Alternatively, a good bicubic reparametrizations scalable by $1/2$ for sprocket layout can be constructed if we split each bicubic into four as shown in Figure 4. However, for the constructions in this paper, we will not need this more complex reparametrization.)

polar layout: Next, we define the C^1 polar reparametrization $\breve{\rho}$ of degree (2,1) which is G^2 due to symmetry. The Bézier coefficients $\breve{\rho}^0_{ij}$, $i = 0..2$, $j = 0, 1$ of one segment of a ring are shown in Figure 5. For $\alpha := 2\pi/N$,

$$\breve{\rho}^0_{00} = (1, 0)\ , \quad \breve{\rho}^0_{10} = (1, \tan(\alpha/2)), \quad \breve{\rho}^0_{20} = (\cos\alpha, \sin\alpha)\ , \quad \breve{\rho}^0_{i1} = \lambda\breve{\rho}^0_{i0}.$$

The coefficients of segment n are defined by rotating by $n\alpha$ about the origin. Unlike $\hat{\rho}$, there is no unique choice of scaling factor λ to obtain the next inner, adjacent ring $\breve{\rho}^{m+1}$ from $\breve{\rho}^m$. To see this, consider the singular map ρ^{sing} of degree $(2, 1)$ with coefficients $\rho^{sing}_{i0} = \breve{\rho}_{i0}$ and $\rho^{sing}_{i1} = (0, 0)$, $i = 0, 1, 2$. The rings $\breve{\rho}^m$ are nested pieces of ρ^{sing} since

$$\breve{\rho}^m(s, t) = \rho^{sing}(s, (1 - \lambda^m)(1 - t) + (1 - \lambda^{m+1})t).$$

The simplest choice, $\lambda = 1/2$, yields equicontraction but results in radially elongated segments. The choice

$$\breve{\lambda} := \frac{1}{1 + 2\sin(\alpha/2)}$$

creates circular and radial boundaries of roughly equal length.

Since the maps $\breve{\rho}^m$ are the parts of one map ρ^{sing}, adjacent rings $\breve{\rho}^m$ and $\breve{\rho}^{m+1}$ join C^∞ after rescaling. Simple direct verification proves also smoothness in the circular direction as summarized in the following lemma.

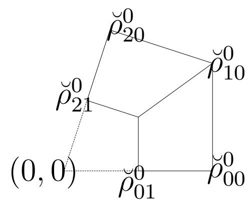

Figure 5: One segment of the G^2 polar reparametrization $\breve\rho$ of degree $(2,1)$.

Lemma 1 *The segments of $\breve\rho^m$ are G^2 connected:*

$$\partial_s^2\breve\rho^m_{n+1}(0,t) = \partial_s^2\breve\rho^m_n(1,t) + k_2\partial_s\breve\rho^m_n(1,t), \qquad k_2 := 2\cos\alpha - 2.$$

4 C^2 guide spline

This section explains the structure of a C^2 spline of total degree d, consisting of N C^2-joined polynomial pieces in total degree Bézier form each piece defined over a unit triangle Δ:

$$\mathbf{g} : \Omega = \Delta \times \mathbb{Z}_N \subset \mathbb{R}^2 \mapsto \mathbb{R}^3.$$

The degree d will be chosen so that the construction is sufficiently flexible to well-approximate boundary data up to the second derivative. [KP0x] will explain in more detail how to set the free parameters of this guide surface g to best match pre-existing C^2 boundary data. The construction is similar to [Pet02]. Piecewise polynomial representation yields more flexibility at a lower degree than the constructions in [Pra97, Rei98, YZ04].

The rays from the center $\mathbf{0} := (0,0)$ through the vertices

$$\mathbf{v}_n := (\cos n\alpha, \sin n\alpha), \quad n = 0,1,\ldots,N-1,$$

subdivide a plane into N sectors $\mathbf{v}_n\mathbf{0}\mathbf{v}_{n+1}$. In each sector, g is represented in total degree, triangular Bézier form with coefficients $\mathbf{g}^n_{ijk}$, $i+j+k=d$, labelled as shown in Figure 6. If the boundary curves of the polynomial pieces match, the well-known conditions for a C^1 join (1) and for a C^2 join (2) are ($\alpha := 2\pi/N$, $\mathsf{c} := \cos\alpha$):

$$\mathbf{g}^{n+1}_{i,d-i-1,1} = -\mathbf{g}^n_{i,1,d-i-1} + 2\mathsf{c}\mathbf{g}^n_{i,0,d-i} + 2(1-\mathsf{c})\mathbf{g}^n_{i+1,0,d-i-1}; \tag{1}$$

$$\begin{aligned}\mathbf{g}^{n+1}_{i,d-i-2,2} = \mathbf{g}^n_{i,2,d-i-2} - 4\mathsf{c}\mathbf{g}^n_{i,1,d-i-1} + 4\mathsf{c}^2\mathbf{g}^n_{i,0,d-i} - 4(1-\mathsf{c})\mathbf{g}^n_{i+1,1,d-i-2}\\ + 8\mathsf{c}(1-\mathsf{c})\mathbf{g}^n_{i+1,0,d-i-1} + 4(1-\mathsf{c})^2\mathbf{g}^n_{i+2,0,d-i-2}.\end{aligned} \tag{2}$$

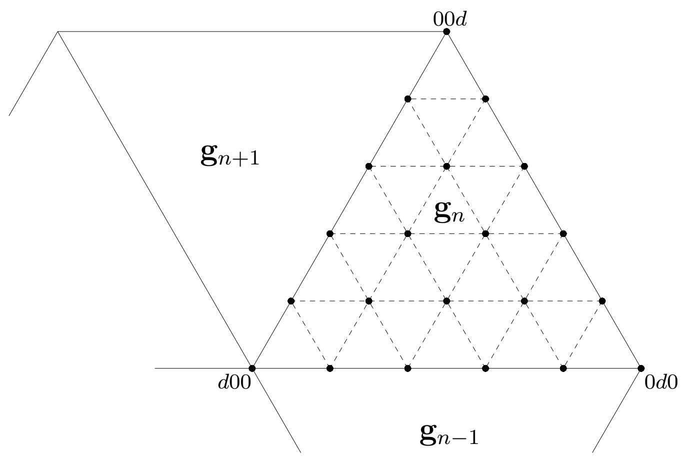

Figure 6: Structure of the piecewise degree d guide spline g that defines the shape near the extraordinary point.

By elementary computations, C^2 smoothness implies the following.

(a) The six coefficients nearest to the extraordinary point, $\mathbf{g}^n_{d00}$, $\mathbf{g}^n_{d-1,1,0}$, $\mathbf{g}^n_{d-1,0,1}$, $\mathbf{g}^n_{d-2,2,0}$, $\mathbf{g}^n_{d-2,1,1}$, $\mathbf{g}^n_{d-2,0,2}$, all have to match a single quadratic polynomial. (in degree-raised form) defined, without loss of generality, by the six coefficients with $n = 0$.

(b) The coefficients $\mathbf{g}^n_{d-3,2,1}$ satisfy the circulant system

$$\mathbf{g}^{n-1}_{d-3,2,1} + 4\mathsf{c}\mathbf{g}^n_{d-3,2,1} + \mathbf{g}^{n+1}_{d-3,2,1} = 2R_n, \tag{3}$$

where

$$R_n := 2\mathsf{c}^2\mathbf{g}^n_{d-3,3,0} + \mathsf{c}\mathbf{g}^n_{d-3,0,3} + 4\mathsf{c}(1-\mathsf{c})\mathbf{g}^n_{d-2,2,0} - 2(1-\mathsf{c})\mathbf{g}^n_{d-2,1,1} + (1-\mathsf{c})\mathbf{g}^n_{d-2,0,2} + 2(1-\mathsf{c})^2\mathbf{g}^n_{d-1,1,0}.$$

(c) If the coefficients $\mathbf{g}^n_{d-3,2,1}$ satisfy (3) then the the coefficients $\mathbf{g}^n_{d-3,1,2}$ are calculated using equation (1).

(d) The coefficients $\mathbf{g}^n_{d-3,3,0}$ can be chosen freely.

Lemma 2 *For* $N \geq 5$, $N \neq 6$,

$$\mathbf{g}^n_{d-3,2,1} = \frac{1}{N}\sum_{i=0}^{N-1}\sum_{j=0}^{N-1}\frac{R_i\cos(n-i)j\alpha}{\cos j\alpha + 2\mathsf{c}}.$$

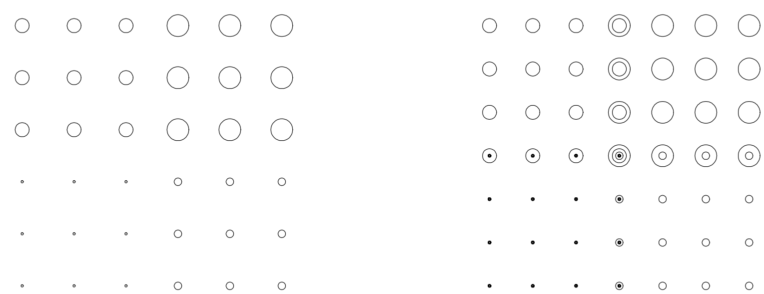

Figure 7: Hermite data merged to define polynomial patch $\mathbf{b}$: (*left*) Second order Hermite data defining a degree (5,5) patch, (*right*) Averaged third order data defining a degree (6,6) patch.

is the unique solution of the system (3).

Proof We apply the discrete Fourier transform (DFT), solve and apply inverse DFT. $|||$

For $N = 3$ the coefficients $\mathbf{g}^n_{i,j,k}$, $i \geq d-3$, are a part of a single cubic polynomial, in degree-raised form. For $N = 4$ there are two additional free coefficients that can be chosen as $\mathbf{g}^0_{d-3,2,1}$, $\mathbf{g}^1_{d-3,2,1}$ and from this an explicit solution can be constructed. For $N = 6$ there is one additional free coefficient that can be chosen as $\mathbf{g}^0_{d-3,2,1}$ and from this an explicit solution can be constructed.

The interplay between the coefficients outside the 3-ring around $\mathbf{0}$, namely between $\mathbf{g}^n_{i,j,k}$, $i < d-3$, is simple: the coefficients $\mathbf{g}^n_{i,d-i,0}$, $\mathbf{g}^n_{i,d-i-j,j}$, $j = 2..d-i-2$, are free and the coefficients $\mathbf{g}^n_{i,1,d-i-1}$, $\mathbf{g}^{n+1}_{i,d-i-1,1}$ are derived by solving the two equations (1) and (2).

5 Pointwise Hermite sampling

This section reviews a simple procedure for creating a quadrilateral Bézier patch $\mathbf{b}$ that matches a map $f : [0..1]^2 \to \mathbb{R}^d$ up to 2nd order at the corners of $[0..1]^2$. For degree (5,5) patch, we construct

$$\mathbf{b} := H(f)$$

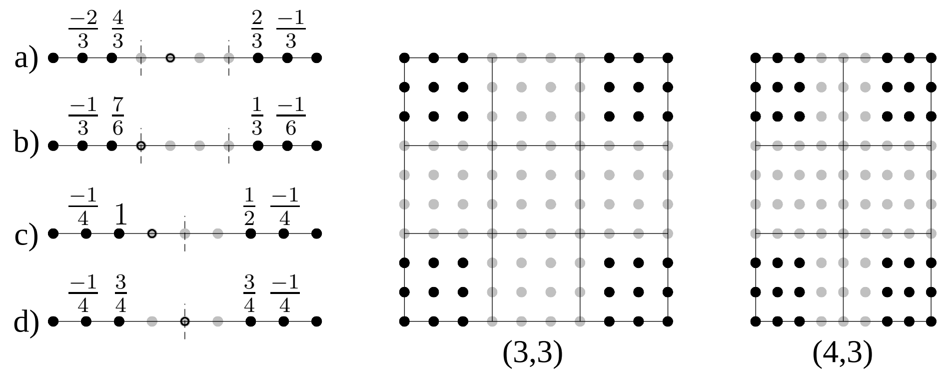

Figure 8: Hermite data merged to define macropatches of degree (i,j) and smoothness $C^{i-1,j-1}$. Formulas a) through d) define unkown Bézier coefficients (*hollow circles*) in terms of the coefficients (*solid black disks*) defined by the H data. Formulas a) and b) define coefficients of a C^2 cubic spline. Formulas c) and d) define coefficients of a C^3 spline of degree 4.

by sampling, at each of the four corners of $[0..1]^2$, the partial derivatives up to second order

$$\begin{array}{ccc} f & \partial_s f & \partial_s^2 f \\ \partial_t f & \partial_s \partial_t f & \partial_s^2 \partial_t f \\ \partial_t^2 f & \partial_s \partial_t^2 f & \partial_s^2 \partial_t^2 f \end{array}$$

and placing the Bézier coefficients that define the partial derivatives into one quadrant of an array as illustrated in Figures 7. To construct, $\mathbf{b} := H(f)$ of degree (6,6), we average the 3rd derivatives in overlapping positions as illustrated in Figure 7, *right*. We can reduce the degree of the sampled patch by choosing it as a spline rather than as a single polynomial. Figure 8 shows several options. Position, first and second derivative at the ends, define a unique C^2 spline consisting of three cubic segments. The formulas for the unknown Bézier points are given in a) and b). Tensoring this procedure yields a Hermite interpolant consisting of nine C^2 connected bicubic patches as shown in Figure 8 (3,3). Similarly, we can construct a C^3 spline consisting of two degree 4 pieces by the formulas c) and d), and combine the univariate to tensored bivariate constructions.

6 Guided patchworks

In this section, the sampled C^2 segments $\mathbf{x}_n^m$, $n = 0, \ldots, N-1$ are joined to form a C^2 (sprocket layout) or G^2 (polar layout) surface rings in $\mathbb{R}^3$. The rings, in turn, are joined into a guided patchwork. First, we consider **polar** case which is simpler than the sprocket layout. We set $\mathbf{x}_n^m := H(\mathbf{g} \circ \breve{\rho}_n^m)$.

Lemma 3 *For $\rho = \breve{\rho}$, the segments $\mathbf{x}_n^m$ and $\mathbf{x}_{n+1}^m$ join C^1 and G^2.*

Proof by Lemma 1 $\breve{\rho}$ is C^1 and hence

$$\partial_s(\mathbf{g} \circ \rho_{n+1}^m)(0,t) = \partial_s(\mathbf{g} \circ \rho_n^m)(1,t) \; .$$

Since k_2 is a constant (hence independent of the transversal direction s),

$$\partial_s^2(\mathbf{g} \circ \rho_{n+1}^m)(0,t) = \partial_s^2(\mathbf{g} \circ \rho_n^m)(1,t) + k_2 \partial_s(\mathbf{g} \circ \rho_n^m)(1,t) \; ,$$

i.e. circularly adjacent segments of $\mathbf{g} \circ \rho$ are C^1 and G^2 connected. Neighboring patches $\mathbf{x}_n^m$ and $\mathbf{x}_{n+1}^m$ match the expansion of $H(\mathbf{g} \circ \rho)$ at the two endpoints and the transversal expansions have the same structure. Since k_2 is a constant (hence independent of t),

$$\partial_s \mathbf{x}_{n+1}^m(0,t) = \partial_s \mathbf{x}_n^m(1,t) \; ,$$
$$\partial_s^2 \mathbf{x}_{n+1}^m(0,t) = \partial_s^2 \mathbf{x}_n^m(1,t) + k_2 \partial_s \mathbf{x}_n^m(1,t)$$

and the claim follows. $|||$

Since adjacent reparametrizations $\breve{\rho}_n^m$, $\breve{\rho}_n^{m+1}$ join C^2, similar arguments show that adjacent rings $\mathbf{x}^m$ and $\mathbf{x}^{m+1}$ are also G^2 connected.

The **sprocket** layout construction, based on $\rho = \hat{\rho}$, samples the guide surface at the corners of the three elementary patches that make up each L-shaped segment. We explain this as a two-step procedure although it is implemented as a single sampling. With $\bar{\mathbf{x}}_n^m := \bigcup H(\mathbf{g} \circ \rho_n^m)$ for a degree $(6,6)$ or a degree $(5,5)$ patchwork arguments as in Lemma 3 show that adjacent L-shapes are C^2 connected (and are internally C^2). But, although actual difference is very small, adjacent rings $\bar{\mathbf{x}}^{m-1}$ and $\bar{\mathbf{x}}^m$ are not even everywhere connected (see Figure 9 *left*). The final $\mathbf{x}^m$ is therefore obtained from $\bar{\mathbf{x}}^m$ by replacing the three outermost layers of Bézier coefficients by a C^2 extension of the patch $\mathbf{x}_n^{m-1}$ (once subdivided to match the granularity), as shown in Figure 9 *middle*, *right*. For $m = 0$, boundary data, if any, are extended.

We summarize.

Lemma 4 *For $\rho = \hat{\rho}$ any finite union of segments and rings $\bigcup_{m \in \mathbb{N}, n \in \mathbb{Z}_N} \mathbf{x}_n^m$ (a* patchwork*) is a C^2 surface. For $\rho = \breve{\rho}$ the union is curvature continuous.*

The $(3,3)$ patchwork is constructed analogously, inheriting C^2-extended data from an outer ring before forming the 3×3 macro-patch.

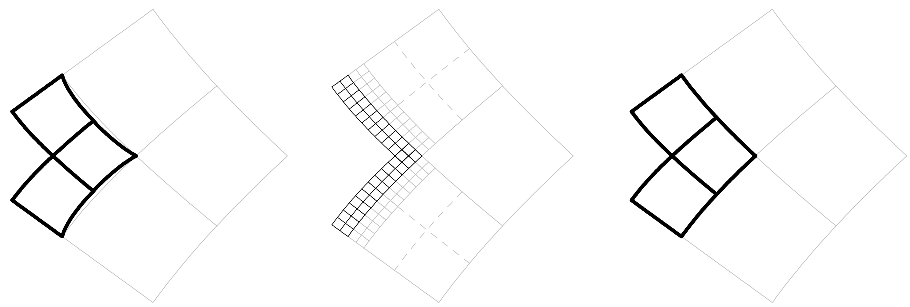

Figure 9: Three steps of C^2 joining the $\hat{\rho}$-sampled patches of a segment.

7 Guided subdivision surfaces

Joining an *infinite* sequence of spline rings results in a surface with subdivision structure (e.g. [RP05, Zo00, Pra98]. Since their construction and, in the polar case, even the layout differs from conventional subdivision, we call these surfaces *guided subdivision surfaces*. In particular, the first step of the subdivision process, constructing a guide, sets guided subdivision apart from the usual procedure of refining meshes. But after the first step, the subdivision process is stationary in the sense that the refinement rules in terms of the control points of the guide surface $\mathbf{g}$ do not change with each step.

Observation 1 *Guided subdivision based on the reparametrizations $\rho = \hat{\rho}$ or $\rho = \breve{\rho}$ is stationary in terms of the control points of the guide surface* $\mathbf{g}$ *and it is a numerically stable procedure.*

Proof Computing the restriction of $\mathbf{g}_n$ to $\lambda\Delta$ involves only convex combinations, hence is numerically stable. Since $\mathbf{g}\circ\rho^m = (\mathbf{g}\lambda^m)\rho^0$, the expression for $H(\mathbf{g}\circ\rho^m)$ and hence of the sampled patches $\mathbf{x}^m$ in terms of the control points of triangular Bézier patches $\mathbf{g}_n\lambda^m$ is independent of the subdivision step. $|||$

To analyze the surface in the limit, we choose the coordinate system so that $\mathbf{x}^{\mathrm{c}} = \mathbf{g}(0,0) = (0,0,0)$. Denote the homogeneous part of degree k with respect to the parameters (u,v) of $\mathbf{g}_n$ by $\mathbf{g}_{n;k}$. Then $\mathbf{g}_{n;k}\lambda^k = \lambda^k\mathbf{g}_{n;k}$ and $\mathbf{x}^1_{n;k} = H(\mathbf{g}_{n;k}\circ\lambda\rho^0) = \lambda^k H(\mathbf{g}_{n;k}\circ\rho^0)$ and we obtain the homogeneous decomposition

$$\mathbf{x}^m_n = \sum_{k=1}^{d} \lambda^{mk}\mathbf{x}^0_{n;k}\ . \tag{4}$$

Expression (4) immediately implies the following.

Theorem 1 *The limit point $m \to \infty$ of $\mathbf{x}^m$ exists and coincides with the center point $\mathbf{x}^{\mathrm{c}}$ of the guide surface.*

Now we turn to the more delicate task of showing that guided subdivision surfaces are C^1 manifolds at $\mathbf{x}^{\mathrm{c}}$ (if the guide surface is such a manifold) and that some of them (namely degree $(6,6)$ sprocket and degree $(4,3)$ polar) are even curvature continuous. It is tempting to use the curvilinear coordinate system defined by ρ and expand $\mathbf{g}$ in terms of ρ to show agreement of the quadratic expansion of $\mathbf{x}$ with the quadratic expansion of $\mathbf{g}$ at $\mathbf{x}^{\mathrm{c}}$. However, the reparametrizations ρ are, by design, singular at the origin and therefore not admissible. In the constructions [Pra97, Rei98, YZ04], this singularity does not matter, since *all* points in the domain are mapped onto the guide surface. Due to sampling, we have to be more careful, but can still use a similar argument. The following lemma states that application of H not only results in approximation but also in reproduction of the lower expansion of the composition.

Lemma 5 *For the patchworks defined in Section 6, (i) $\mathbf{x}^m_{n;1} = \mathbf{g}_{n,1} \circ \rho^m$. For degree $(6,6)$ sprocket and degree $(4,3)$ polar patchworks $\mathbf{x}$, additionally (ii) $\mathbf{x}^m_{n;1} + \mathbf{x}^m_{n;2} = (\mathbf{g}_{n,1} + \mathbf{g}_{n,2}) \circ \rho^m$.*

Proof By definition, degree $\mathbf{g}_{n,k} = k$, and the degree of ρ^m is either $(3,3)$ or $(2,1)$. Therefore,

(i) degree$(\mathbf{g}_{n,1} \circ \rho^m) =$ degree$(\rho^m) \leq$ degree$(\mathbf{x}^m_{n;1})$.

(ii) degree$((\mathbf{g}_{n,1} + \mathbf{g}_{n,2}) \circ \rho^m) = 2$ degree$(\rho^m) \leq$ degree$(\mathbf{x}^m_{n;1} + \mathbf{x}^m_{n;2})$. |||

That is, guided subdivision reproduces compositions with linear and quadratic guide surfaces. We denote by

$$\pi_{>k}(s_1, \ldots, s_i; t_1, \ldots, t_j)$$

(piecewise) polynomial terms of degree greater than k in each of the variables $s_1, \ldots, s_i$ and with the coefficients depending on $t_1, \ldots, t_j$. If the coefficients are constant, we write $\pi_{>k}(s_1, \ldots, s_i)$.

For the remainder, we assume that the tangent planes of $\mathbf{g}$ are well-defined in the vicinity of $(0,0)$.

Theorem 2 *For the patchworks $\mathbf{x}$ defined in Section 6, a unique limit of the tangent planes of the surface rings $\mathbf{x}^m$ exists as $m \to \infty$ and equals the tangent plane of the guide surface at $\mathbf{x}^{\mathrm{c}}$.*

Proof We define $\mathbf{n}^m := \partial_s \mathbf{x}^m \times \partial_t \mathbf{x}^m$ and note that $\mathbf{g}_{n;k}$ depends on n only for $k > 2$, i.e. we can define $\mathbf{n}^m$ below independent of n. From (4) and Lemma 5 (i),

$$\mathbf{n}^m(s,t) = \lambda^{2m}\big(\partial_s(\mathbf{g}_{.;1} \circ \rho^0) \times \partial_t(\mathbf{g}_{.;1} \circ \rho^0)\big)(s,t) + \lambda^{rm}\pi_{\geq 0}(s,t;\lambda)\ ,\ r \geq 3\ .$$

Then

$$\frac{\mathbf{n}^m}{||\mathbf{n}^m||} = \frac{\partial_s(\mathbf{g}_{.;1} \circ \rho^0) \times \partial_t(\mathbf{g}_{.;1} \circ \rho^0) + \lambda^{(r-2)m}\pi_{\geq 0}(s,t;\lambda)}{||\partial_s(\mathbf{g}_{.;1} \circ \rho^0) \times \partial_t(\mathbf{g}_{.;1} \circ \rho^0) + \lambda^{(r-2)m}\pi_{\geq 0}(s,t;\lambda)||}$$

so that $\lim_{m\to\infty} \frac{\mathbf{n}^m}{||\mathbf{n}^m||}$ is normal to the tangent plane of $\mathbf{g}$ at $\mathbf{x}^c$. |||

We may now assume that the coordinate system (x, y, z) in $\mathbb{R}^3$ is chosen so that

$$\mathbf{x}^c = (0,0,0) \text{ and the tangent plane at } \mathbf{x}^c \text{ is } \{z = 0\}. \tag{5}$$

Since $\hat{\rho}$ is injective (see e.g. [PR98]) and the injectivity of $\breve{\rho}$ follows directly from its definition, the projection $\mathbf{x} \to (x, y)$ is locally injective near $\mathbf{x}^c$. Then standard arguments based on the mean value theorem show that the inverse map is C^1 at the origin (cf. [RP05] p.105 (4)). Hence the following theorem holds.

Theorem 3 *The guided subdivision surface $\mathbf{x}$ is C^1 at $\mathbf{x}^c$ and the tangent plane of $\mathbf{x}$ at $\mathbf{x}^c$ coincides with that of guide surface.*

The rest of this Section is devoted to the proof of curvature continuity for degree $(6,6)$ sprocket and degree $(4,3)$ polar guided subdivision surfaces.

Definition 1 (curvature continuity) *Let $\mathbf{f} : \mathbb{R}^2 \to \mathbb{R}^3$ be tangent plane continuous at $\mathbf{f}_0 := \mathbf{f}(0,0)$. We choose a coordinate system (5) so that the tangent plane at $\mathbf{f}_0 = (0,0,0)$ is $\{z = 0\}$. Assume further that for every $(s,t) \neq (0,0)$ there exists a unique (elliptic or hyperbolic)* osculating paraboloid $\mathbf{q} := (q_0, \ldots, q_5)^T$ anchored at (s,t)*, i.e. with the q_i continuous functions of (s,t) such that*

$$\text{for } (x,y,z) = \mathbf{f}(s+\bar{s}, t+\bar{t}), \qquad z = (x^2, xy, y^2, x, y, 1)\mathbf{q}(s,t) + \pi_{>2}(\bar{s},\bar{t}; s,t). \tag{6}$$

Then the surface $\mathbf{f}$ *is* curvature continuous *at* $\mathbf{f}_0$ *if the anchored osculating paraboloids have a unique limit at* $\mathbf{f}_0$.

The advantage of fixing the coordinate system of the osculating paraboloid at (s,t) over defining it at $(s+\bar{s}, t+\bar{t})$ as is common in differential geometry is that the anchored osculating paraboloid does not vary if data are sampled from the paraboloid (see Figure 10).

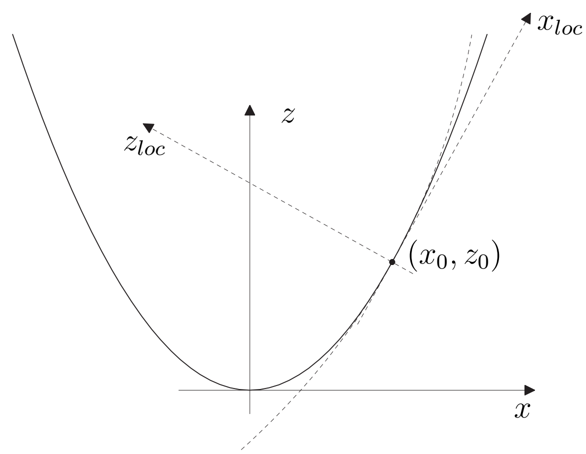

Figure 10: The osculating parabolas (*dashed*) vary with the local coordinate system at points x_{loc}, z_{loc} on an anchored osculating parabola (*solid*).

Theorem 4 (curvature continuity) *sprocket degree* $(6,6)$ *and polar degree* $(4,3)$ *guided subdivision surfaces* $\mathbf{x}$ *are curvature continuous at the extraordinary point* $\mathbf{x}^{\mathrm{c}}$ *if the guide surface* $\mathbf{g}$ *has a unique osculating paraboloid* $\mathbf{q}$ *at* $\mathbf{x}^{\mathrm{c}}$. *The limit of the osculating paraboloids of* $\mathbf{x}$ *at* $\mathbf{x}^{\mathrm{c}}$ *is* $\mathbf{q}$.

Proof We fix a coordinate system (5) so that, near $\mathbf{x}^{\mathrm{c}}$,

$$\mathbf{g} = (u + \pi_{>1}(u,v), v + \pi_{>1}(u,v), au^2 + buv + cv^2 + \pi_{>2}(u,v)) \ .$$

With $(s+\bar{s}, t+\bar{t})$ a point near $(s,t) \in \Sigma^0$, we expand ρ_n^0 to second degree at (s,t)

$$\begin{aligned}
\rho_n^0 =& (u(s+\bar{s}, t+\bar{t}), v(s+\bar{s}, t+\bar{t})) \\
=& (\bar{u}(\bar{s},\bar{t};s,t) + \pi_{>2}(\bar{s},\bar{t};s,t), \bar{v}(\bar{s},\bar{t};s,t) + \pi_{>2}(\bar{s},\bar{t};s,t)) \ ; \\
\bar{u}(\bar{s},\bar{t};s,t) :=& u_0 + h_0\bar{s} + h_2\bar{t} + h_4\bar{s}^2 + h_6\bar{s}\bar{t} + h_8\bar{t}^2, \\
\bar{v}(\bar{s},\bar{t};s,t) :=& v_0 + h_1\bar{s} + h_3\bar{t} + h_5\bar{s}^2 + h_7\bar{s}\bar{t} + h_9\bar{t}^2 \ .
\end{aligned}$$

Note that u_0, v_0 and h_i are piecewise polynomials in s and t. Since ρ^0 is injective on the compact domain $\Sigma^0 \times \mathbb{Z}_N$, $h_0h_3 - h_1h_2 \geq const > 0$. By the homogeneous expansion (4),

$$\mathbf{x}_n^0 = \sum_{k=1}^{d} l^k \mathbf{x}_{n;k}^0, \qquad l := \lambda^m,$$

and by Lemma 5 (ii),

$$\begin{aligned}\mathbf{x}_n^m &= l(\mathbf{g}_{n;1}\circ\rho_n^0) + l^2(\mathbf{g}_{n;2}\circ\rho_n^0) + l^3(\dots)\\ &= (l\bar u + l^2E_1, l\bar v + l^2E_2, l^2(a\bar u^2 + b\bar u\bar v + c\bar v^2) + l^3E_3) + \pi_{>2}(\bar s,\bar t;s,t,l)\ ,\end{aligned} \tag{7}$$

where E_k are some polynomials of total degree 2 in $(\bar s,\bar t)$ with coefficients depending on s, t, l. This expression for $\mathbf{x}_n^m = (x,y,z)$ is substituted into the anchored osculating paraboloids of $\mathbf{x}$. Near $\mathbf{x}^c$, with $\mathbf{q} := (a,b,c,0,0,0)^T$ constant, independent of (s,t) and $\mathbf{d} := (d_0,\dots,d_5)^T$, each term depending on (s,t), the osculating paraboloid has the form

$$z = (x^2, xy, y^2, x, y, 1)(\mathbf{q}+\mathbf{d}). \tag{8}$$

Equating the coefficients of 1, $\bar s$, $\bar t$, $\bar s^2$, $\bar s\bar t$, $\bar t^2$ to 0, we get the system of six linear equations in the six unknowns $d_j(s,t)$,

$$M\mathbf{d} = \mathbf{r} \tag{9}$$

where the first three columns of M have a factor l^2, the next two a factor l and M is of full rank apart from $(0,0)$ since det$M = -l^8((h_0h_3 - h_1h_2)^4 + \pi_{>8}(l;s,t) \neq 0$. Since the right hand side $\mathbf{r}$ has a factor l^3, hence vanishes faster than the matrix entries, $\lim_{l\to 0} d_j = 0$. This satisfies Definition 1. |||

The lower degree bound for curvature continuous subdivision surfaces [Rei96] applies to guided subdivision surfaces with sprocket layout; the curvature continuous polar surfaces of degree $(4,3)$ do not contradict this bound since the patch layout is different from the one assumed in [Rei96]. The layout allows reducing the radial degree to 3 and replacing C^2 continuity by geometric G^2 continuity allows reducing the circular degree to 4.

To see that curvature continuous guided subdivision surfaces are C^2 from the point of view of differential geometry, we consider a local parametrization $(x,y,h(x,y))$ of the surface at $\mathbf{x}^c$. The height function h is C^1 by Theorem 3 and the partial derivatives h_x, h_y are C^1 apart from $(0,0)$, by construction (and since the limit osculating paraboloid $\mathbf{q}$ is anchored at $\mathbf{x}^c$ and therefore, in particular, the constant component of $\mathbf{q}$ vanishes faster than the other q_i). The G^2 connection for polar layout does not create a problem since the G^2 constraints reparametrize a C^2 join. Theorem 4 shows that first partial derivatives of h_x, h_y are well defined as $\lim_{(x,y)\to(0,0)}$. The mean value theorem implies that h_x, h_y are C^1 at the origin. Hence h is C^2 at the origin.

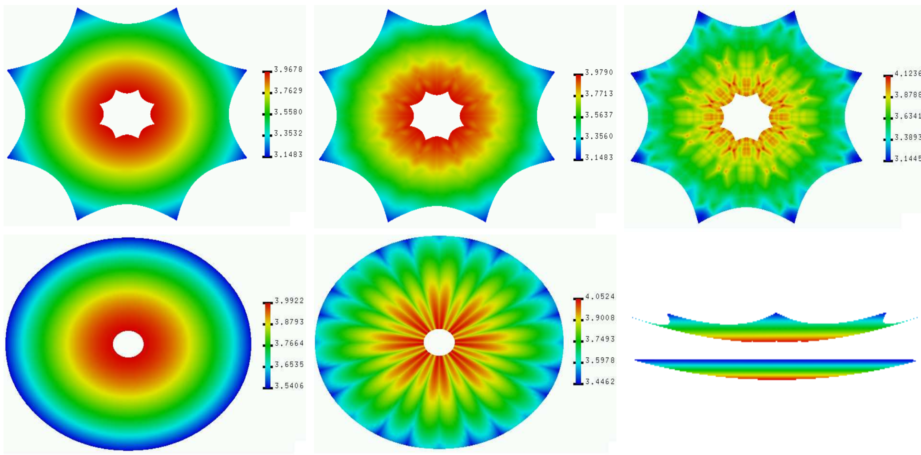

Figure 11: Gauss curvature shading. (*top*) sprocket layout subdivision of degree (6,6) (*left*), (5,5) (*middle*) and (3,3) (*right*). (*bottom*) Polar layout subdivision of degree (4,3) (*left*), and (3,3) (*middle*). (*bottom,right*) juxtaposes the sprocket (top) and polar (bottom) C^2 surfaces.

8 Curvature estimates for lower-degree guided subdivision

Here we bound the curvature at the extraordinary point when the degree of $\mathbf{x}$ is chosen lower than $(6,6)$ in the sprocket case and $(4,3)$ in the polar case. The trade-off between quality and degree will be discussed in more detail in a later report although Figure 11 gives a first impression. Lower degree is often required by an application and we will give an algorithm for practically computing the bounds. Also, the discussion highlights the computational value of introducing anchored osculating paraboloids.

Theorem 5 *Guided subdivision surfaces of degree (3,3) and higher have bounded curvature at the extraordinary point.*

Proof We follow the proof of Theorem 4 but replace formula (7) by

$$\begin{aligned}\mathbf{x}_n^m =&(l\bar{u} + l^2E_1, l\bar{v} + l^2E_2, l^2\bar{z} + l^3E_3) + \pi_{>2}(\bar{s},\bar{t};s,t,l)\ ,\\ \bar{z} :=& \tilde{h}_0 + \tilde{h}_1\bar{s} + \tilde{h}_2\bar{t} + \tilde{h}_3\bar{s}^2 + \tilde{h}_4\bar{s}\bar{t} + \tilde{h}_5\bar{t}^2\end{aligned} \tag{10}$$

and the paraboloid by $z = (x^2, xy, y^2, x, y, 1)\mathbf{d}$ since Lemma 5 (ii) may not hold and no osculating paraboloid exists anchored at $\mathbf{f}_0$ whose perturbation we would consider. We obtain a constraint matrix M of full rank and with the same factors of l as (9). However, the right hand side $\mathbf{r}$ now has a factor of l^2, enough only to conclude

$$\lim_{l\to 0} d_j = 0 \text{ for } j = 3,4,5.$$

We will compute bounds on d_0, d_1, d_2 by applying Cramer's rule. Since the factor l^2 appears both in $\mathbf{r}$ and the relevant first three columns of M, we can remove the factors from the matrix and the right hand and write them respectively as

$$\begin{pmatrix} u_0^2+. & u_0v_0+. & v_0^2+. & u_0+. & v_0+. & 1 \\ 2h_0u_0+. & h_0v_0+h_1u_0+. & 2h_1v_0+. & h_0+. & h_1+. & 0 \\ 2h_2u_0+. & h_2v_0+h_3u_0+. & 2h_3v_0+. & h_2+. & h_3+. & 0 \\ h_0^2+2h_4u_0+. & h_0h_1+h_4v_0+h_5u_0+. & h_1^2+2h_5v_0+. & h_4+. & h_5+. & 0 \\ 2h_0h_2+2h_6u_0+. & h_0h_3+h_1h_2+h_6v_0+h_7u_0+. & 2h_1h_3+2h_7v_0+. & h_6+. & h_7+. & 0 \\ h_2^2+2h_8u_0+. & h_2h_3+h_8v_0+h_9u_0+. & h_3^2+2h_9v_0+. & h_8+. & h_9+. & 0 \end{pmatrix}, \begin{pmatrix} \tilde{h}_0+. \\ \tilde{h}_1+. \\ \tilde{h}_2+. \\ \tilde{h}_3+. \\ \tilde{h}_4+. \\ \tilde{h}_5+. \end{pmatrix} \quad (11)$$

where $+.$ is a shorthand for polynomial terms $\pi_{>0}(l;s,t)$ that will vanish as $l \to 0$. Elimination of the first row and multilinearity of determinants yields a simpler system

$$\begin{pmatrix} 0+. & 0+. & 0+. & h_0+. & h_1+. \\ 0+. & 0+. & 0+. & h_2+. & h_3+. \\ h_0^2+. & h_0h_1+. & h_1^2+. & h_4+. & h_5+. \\ 2h_0h_2+. & h_0h_3+h_1h_2+. & 2h_1h_3+. & h_6+. & h_7+. \\ h_2^2+. & h_2h_3+. & h_3^2+. & h_8+. & h_9+. \end{pmatrix} \begin{pmatrix} d_0 \\ d_1 \\ d_2 \\ d_4 \\ d_5 \end{pmatrix} = \begin{pmatrix} \tilde{h}_1+. \\ \tilde{h}_2+. \\ \tilde{h}_3+. \\ \tilde{h}_4+. \\ \tilde{h}_5+. \end{pmatrix} . \quad (12)$$

Since $h_0h_3 - h_1h_2$ is bounded away from zero due to the injectivity of ρ, det$M = (h_0h_3 - h_1h_2)^4 + . \geq const > 0$ and $D :=$ det $\lim_{l\to 0} M$ is well-defined. Let D_i be the determinant of the matrix obtained by replacing the $(i+1)$th column of M by r and by taking the limit for $l \to 0$ to drop the terms $+.$, we have by Cramer's rule

$$d_i = \frac{D_i}{D}\ ,\ i = 0,1,2\ .$$

Since the denominator is well-defined, the d_i are bounded. $|||$

The practical calculation of the bounds on the coefficients d_0, d_1 and d_2 of the osculating paraboloid is simplified since D and D_i share factors $h_0h_3 - h_1h_2$. Specifically, we compute as follows.

(i) Bounding the coefficients d_0, d_1, d_2 for functionns $f_1 := u^2$, $f_2 := uv$, $f_3 := v^2$ in turn yields nine intervals that allow computing the bounds for any function $f = \gamma_1 u^2 + \gamma_2 uv + \gamma_3 v^2$.

(ii) If (x,y,z) is an *orthogonal* coordinate system in $\mathbb{R}^3$ with $\mathbf{x}^c = (0,0,0)$, tangent plane $\{z = 0\}$ at $\mathbf{x}^c$ and $\mathbf{g} = (e_{11}u + e_{12}v + \pi_{>1}(u,v), e_{21}u + e_{22}v + \pi_{>1}(u,v), au^2 + buv + cv^2 + \pi_{>2}(u,v))$, then the bounds of coefficients d'_k of osculating paraboloid in such system are calculated from the previous bounds of coefficients d_k as

$$\begin{aligned} d'_0 =& d_0e_0^2 + d_1e_0e_1 + d_2e_1^2 \ , \ d'_2 = d_0e_2^2 + d_1e_2e_3 + d_2e_3^2 \\ d'_1 =& 2d_0e_0e_2 + d_1(e_0e_3 + e_1e_2) + 2d_2e_1e_3 \ , \end{aligned} \tag{13}$$

where $\left(\begin{smallmatrix} e_0 & e_2 \\ e_1 & e_3 \end{smallmatrix}\right) := \left(\begin{smallmatrix} e_{11} & e_{12} \\ e_{21} & e_{22} \end{smallmatrix}\right)^{-1}$.
(iii) To bound *Gaussian and mean curvatures*, we observe that for an osculating paraboloid $(x, y, d'_0x^2 + d'_1xy + d'_2y^2)$ the mean H and Gaussian K curvatures at the origin $(0, 0, 0)$ are

$$H = d'_0 + d'_2 \ , K = 4d'_0d'_2 - d'^2_1 \ .$$

substituting formulas (13), we get

$$\begin{aligned} H =& (e_0^2 + e_2)^2d_0 + (e_0e_1 + e_2e_3)d_1 + (e_1^2 + e_3^2)d_2 \ , \\ K =& (e_0e_3 - e_1e_2)^2(4d_0d_2 - d_1^2) \ . \end{aligned} \tag{14}$$

For Gaussian curvature K, we get a tighter estimate if, in formula (14), the part $4d_0d_2 - d_1^2$ is precomputed with respect basis functions f_1, f_2, f_3. The result are, consistent with [Pet01], six precomputed intervals and nine intervals for H.
(iv) Defining $f_1 := u^2 + v^2$, $f_2 := uv$, $f_3 := v^2$ gives an immediate impression of how guided subdivision reproduces canonical elliptic, hyperbolic and parabolic shapes. We list some bounds on the Gaussian curvature for these shapes when $N = 8$.

	$(3,3)^{CC}$	$(5,5)^{CC}$	$(3,3)^{pol}$
$u^2 + v^2$	$[3.87501, 4.22213]$	$[3.96505, 4.02945]$	$[3.98505, 4.03352]$
uv	$[-1.06493, -0.96478]$	$[-1.00426, -0.99261]$	$[-1.05229, -0.97047]$
v^2	$[-0.15738, 0.15644]$	$[-0.02054, 0.02241]$	$[-0.09641, 0.05184]$

9 The accelerated bicubic guided C^2 scheme

We consider a sampling scheme that is no longer stationary, since, in each step, we sample with increasing density. Each quad in $\mathbf{S}^0$ is evenly subdivided into 4^m subquads at level m and H is applied over each subquad creating 4^m of pieces of 3×3 bicubic patches that are joined C^2 as explained in Section 5. We call this scheme *accelerated* bicubic and observe that the sampled data will be sufficiently dense after a couple of steps to meet the bounds needed for the proof below so that we can switch to a fixed density, pseudostationary sampling.

Theorem 6 *Accelerated bicubic guided subdivision surfaces* $\mathbf{x}$ *are curvature continuous at* $\mathbf{x}^c$. *Moreover, the limit of osculating paraboloids of* $\mathbf{x}$ *at* $\mathbf{x}^c$ *coincide with that of guide surface* $\mathbf{g}$.

Proof The proof follows that of Theorem 5. By Theorem 2, accelerated subdivision inherits the tangent plane of the guide surface at $\mathbf{x}^c$. To show curvature continuity, we observe that if a polynomial $\mathbf{g} \circ \rho : [0..1]^2 \to \mathbb{R}$ is bicubically sampled at the corners (s,t) of 4^m subquads to define a segment $\mathbf{x}_n^m$ consisting of 4^m patches then, for a fixed $\epsilon > 0$ and m sufficiently large, the value and partial derivatives of $\mathbf{g} \circ \rho$ and $\mathbf{x}_n^m$ differ everywhere by less than ϵ. Since the domain is compact, also the functions h_i, $\tilde{h}_j$ in (12) deviate from their value at the corners by less than a fixed ϵ and all expressions $(+.)$ are bounded and converge to zero with m. With $\mathbf{q} := (a,b,c,0,0,0)^T$ the osculating paraboloid of $\mathbf{g}$ at $(0,0)$, d_i converges to q_i: $\lim_{l\to 0} d_0 = a$, $\lim_{l\to 0} d_1 = b$, $\lim_{l\to 0} d_2 = c$. |||

As in Section 7, one can argue that the accelerated subdivision surfaces are C^2 in the sense of differential geometry.

10 Rational guided subdivision

If the guide surface is rational, e.g. $\mathbf{g} := (f_1/f_4, f_2/f_4, f_3/f_4)$, we can either sample in $\mathbb{R}^3$ (and all proofs and theorems apply to the resulting polynomial guided subdivision surface) or, we sample the homogeneous guide (f_1, f_2, f_3, f_4) in $\mathbb{R}^4$ and project the result to $\mathbb{R}^3$. The latter allows reproducing, e.g. the sphere, exactly. As a stationary construction, this differs from the approach in [MWW01] (which is akin to accelerated scheme in that the density increases at the poles) and from [SZSS98, SZBN03].

11 Conclusions

This paper defined *local subdivision constructions* that, for practical applications, would be embedded in a larger scheme that separates local subdivision regions by constructing and pairwise blending primary surfaces. Such schemes, for example one or more steps of Catmull-Clark subdivision, are discussed in [KP0x]. [KP0x] also explains how to choose the free parameters of the guide surface $\mathbf{g}$ to transition from primary surfaces to the local subdivision surfaces without introducing unnecessary shape artifacts, and how to stop the subdivision process to fill in the remaining multi-sided hole with polynomial pieces of moderate degree.

Here we established that any finite number of surface rings join to form a C^2 surface (2-manifold with boundary) with a gap at the center; and, in the limit, the construction yields curvature continuous subdivision surfaces of low degree. A generalization to higher-order smoothness looks straightforward although the details, e.g. the choice of reparametrizations, requires attention.

Acknowledgement: This work was supported by NSF Grant CCF-0430891.

References

[KP0x] K. Karčiauskas and J. Peters. Finite Guided Patchworks. *Computer Aided Geometric Design,* to be submitted.

[MWW01] G. Morin and J. Warren and H. Weimar. A Subdivision Scheme for Surfaces of Revolution. *Computer Aided Geometric Design*, 18:483–502,2001.

[Pet02] J. Peters. C^2 free-form surfaces of degree (3,5). *Computer Aided Geometric Design*, 19(2):113–126, 2002.

[Pet01] J. Peters and G. Umlauf. Computing curvature bounds for bounded curvature subdivision. *Comput. Aided Geom. Design*, 18:455–462, 2001.

[PR98] J. Peters and U. Reif. Analysis of generalized B-spline subdivision algorithms. *SIAM J of Numer. Anal.*, 35(2):728–748, April 1998.

[Pra97] H. Prautzsch. Freeform splines. *Comput. Aided Geom. Design*, 14(3):201–206, 1997.

[Pra98] H. Prautzsch. Smoothness of subdivision surfaces at extraordinary points. *Adv. in: Comp. Math.*, 9:377–390, 1998.

[Rei96] U. Reif. A degree estimate for subdivision surfaces of higher regularity. *Proc. Amer. Math. Soc.*, 124(7):2167–2174, 1996.

[Rei98] U. Reif. TURBS—topologically unrestricted rational B-splines. *Constr. Approx.*, 14(1):57–77, 1998.

[RP05] U. Reif and J. Peters. Structural analysis of subdivision surfaces – a summary. In K. Jetter et al., editor, *Topics in Multivariate Approximation and Interpolation*. Springer, submitted.

[SZSS98] T W. Sederberg and J Zheng and D Sewell and M Sabin, Non-Uniform Recursive Subdivision Surfaces, *Proceedings of SIGGRAPH 98*, ed. M Cohen, 387–394,1998.

[SZBN03] T. W. Sederberg and J Zheng and A Bakenov and A Nasri, T-splines and T-NURCCs, *ACM Transactions on Graphics*,22(3), 477–484, 2003.

[YZ04] L. Ying and D. Zorin. A simple manifold-based construction of surfaces of arbitrary smoothness. *ACM ToG*, 23(3), pages 271–275, 2004.

[Zo00] D. Zorin. Smoothness of stationary subdivision on irregular meshes. *Constr. Approx.*, 16(3):359–397, 2000.